Study on preparation and corrosion property of ultrafine grinding catalytic internal electrolytic filler

Ajun Wan[a,*], Yunpeng Wu[a], Jiucheng Wang[a,b], Runqiu Tu[a], Luting Pan[a], Xiaolei Qi[a], Yixuan Liu[a]

[a]*Institute of New Rural Development, Tongji University, Shanghai 201804, China, emails: wanajun@tongji.edu.cn (A. Wan), dxwyp@tongji.edu.cn (Y. Wu), 394138641@qq.com (J. Wang), 1733004@tongji.edu.cn (R. Tu), lutingpan@163.com (L. Pan), 630330376@qq.com (X. Qi), 1939849239@qq.com (Y. Liu)*
[b]*Tus-Design Group Co. Ltd., Jiangsu Suzhou 21500, China*

ABSTRACT

In order to solve the bottleneck of internal electrolysis technology, ultrafine grinding catalytic internal electrolytic fillers were prepared by powder metallurgy method. Under the initial conditions of ball-to-powder weight ratio 10:1, taking particle size, particle size distribution and particle morphology as evaluation criteria, the effects of ball milling time, ball milling speed and absolute ethanol addition on the effect of powder ball milling were studied by single factor test and orthogonal test. The results show that the optimal parameters of the ball milling process are ball milling time of 20 h, ball milling speed of 300 rpm and absolute ethanol addition of 50% (by total powder mass). The influence of the three factors on the ball milling effect is extremely significant, and there is an interaction between the three. Finally, the corrosion values at different pH levels were obtained by potentiodynamic scanning of self-made internal electrolytic fillers and two kinds of commercial internal electrolytic fillers. By calculating the corrosion rate, the optimum pH value for the reaction of self-made internal electrolytic filler is 3. The corrosion rate of self-made internal electrolytic filler is the fastest, the reaction rate is the highest, and the passivation and bonding phenomenon are alleviated.

Keywords: Internal electrolytic filler; Powder metallurgy; Electropotential polarization curve; Corrosion performance

1. Introduction

Internal electrolysis is a technique in which the pollutants are removed by oxidation, reduction, flocculation and adsorption by using the redox reaction on the surface of the electrode and the active intermediates (such as O^{2-}, H_2O_2, $^{\bullet}OH$, etc.) under the action of the iron carbon primary battery [1,2]. At present, it is widely used in the pretreatment, decolorization and heavy metal wastewater treatment of refractory biodegradable organic wastewater [3,4] from industries such as paper making [5], printing and dyeing [6], pharmaceutical [7], tobacco [8], petrochemical [9].

The pretreatment of refractory industrial wastewater by internal electrolysis technology still has some problems in some practical projects, such as filler passivation, filler agglomeration, sludge production and so on. To solve these problems, the current improvement measures mainly include the following aspects. (1) Study on internal electrolytic reactors. Song et al. [10] developed a new internal electrolysis system in which iron and carbon were placed separately and connected by wires. The results showed that the removal rate of p-nitrophenol was obviously higher than that of non-correlation. And compared with iron-carbon mixtures, the iron consumption of both was equal. (2) Study

* Corresponding author.

on internal electrolysis reactor. At present, the fixed-bed reactor is widely used in domestic industrial wastewater pretreatment projects by internal electrolysis technology, and the phenomenon of packed layer solidification generally exists in this kind of reactor. In recent years, researchers at home and abroad have begun to develop new internal electrolysis reactor based on traditional fixed bed, including fluidized bed reactor, rotary drum reactor and so on. (3) Internal electrolysis is combined with other technologies. Lu et al. [11] used micro-electrolysis as pretreatment technology, combined with O–A–O biochemical process to treat chemical wastewater. The experimental results showed that micro-electrolysis could remove sulfur ion and chroma better, and the B/C ratio increased from 0.17 to 0.32. However, the preparation of a new type of filler with self-passivation, slower knotting, and long life has not been studied in detail. Based on this, this study proposes to prepare a new type of internal electrolytic filler by reducing the particle size and increasing the uniformity of distribution. And this method is powder metallurgy (PM).

PM is a process technology that uses metal powder (or a mixture of metal powder and non-metallic powder) as a basic raw material to make metal materials, composite materials and various types of products through processes including mixing, pressing, sintering, shaping, oil immersion, etc. [12]. PM method is frequently combined with ball milling technique which includes repeated cold welding, fracture and rewelding of powder particles in a high-energy ball mill, and therefore it enables to obtain fine and homogeneous dispersion of brittle phase in the ductile matrix [13]. Studies have shown that ball-to-powder weight ratio, ball milling speed, ball milling time, process control agent (PCA) and other process parameters have an effect on the final structure and morphology of the powder [14–18]. Therefore, the influence of the above factors on the effect of the filler should be considered in the preparation of the filler.

The method for preparing ultrafine powder catalytic internal electrolysis packing by PM introduced in this paper obtained internal electrolytic filler with fine particle size and uniform distribution of iron and carbon by studying the ball milling speed, ball milling time and absolute ethanol addition. Further analysis of the corrosion performance of the self-made internal electrolytic fillers proves that the purpose of improving the number of corrosion micro-cells on the surface area of the unit filler and improving the performance is achieved. The preparation method of the novel high-efficiency internal electrolytic filler expands the preparation method of the filler, so that the electrolytic packing and the passivation phenomenon are alleviated, the service life is prolonged and the treatment effect is kept stable. The new filler can be used for the treatment of industrial wastewater, especially pulping wastewater [19].

2. Materials and methods of experiment

2.1. Experimental materials

The specifications and origins of raw materials used in the experiment are shown in Table 1.

2.2. Experimental method

Based on the preparation and characterization of traditional iron-carbon internal electrolytic fillers and the influencing factors of catalytic internal electrolysis process [20–22], the electrolytic fillers in ultrafine powders were prepared by PM. (1) The original powder (mixed powder with a total mass of 50 g according to the mass percentage of Fe-6C-0.5Cu-0.5Mn) was refined and mixed uniformly by a QM-3SP4 planetary ball mill. The ball mill and the grinding ball are made of stainless steel, the volume of the ball mill is 500 mL, and the ball to material ratio is 10:1. The grinding balls are, respectively, selected from stainless steel balls with diameters of 6, 10 and 15 mm, and the mass ratio is 1:3:1. (2) The mixed powder was pressed into a green body having a certain shape by using an FLS-10 manual double-column hydraulic press. The pressing pressure was 200 MPa and the holding time was 10 min. (3) The green body was placed in an industrial mesh belt sintering furnace for sintering. Then taking particle size, particle size distribution and particle morphology as evaluation criteria, the effects of ball milling time, ball milling speed and absolute ethanol addition on ball milling effect were investigated through single factor and orthogonal experiments, and the optimum preparation conditions were obtained. The surface morphology of powder and internal electrolytic filler was observed by scanning electron microscopy, and the particle size distribution was measured by laser particle size analyzer.

Potentiodynamic polarization curves of self-made fillers in NaCl solutions with different pH values were obtained by potentiodynamic scanning. Corrosion rate was calculated according to Eq. (1). At the same time, the corrosion properties of self-made ultra-fine powder inner electrolytic filler and traditional inner electrolytic filler were compared under the same conditions.

$$v = \frac{M}{nF} \times i_{\text{coor}} \tag{1}$$

Here v is the corrosion rate of metal in g/(m²h); M is the relative atomic mass of metal in g/mol; F is the Faraday

Table 1
Specification and origin of experimental raw materials

Powder type	Purity	D_{50}/μm	Place of origin
Water atomized iron powder	≥99.7%	68.134	Changsha
Natural graphite powder	≥99.9%	3.885	Shanghai
Electrolytic copper	≥99.5%	32.574	Changsha
Electrolytic manganese powder	≥99.5%	15.631	Changsha

constant (96485 s A/mol); n is the number of gain and loss electrons in the equation of electrode reaction; and i_{coor} is the corrosion current density in $\mu A/cm^2$.

3. Experimental results and analysis

3.1. Characteristics of experimental raw materials

3.1.1. Particle size distribution characteristics

The particle size and size distribution of the powders largely determine the performance of the prepared materials, and also affect the difficulty of the preparation process [23]. Therefore, the particle size of the four raw materials used in the experiment was analyzed. The results are shown in Fig. 1 and the particle size characteristic parameters are shown in Table 2.

Fig. 1 shows that the particle size of iron powder (Fig. 1a) was between 20 and 200 μm, and the peak value was about 80 μm. There were two peaks in the graphite particle size distribution (Fig. 1b), about 5 and 40 μm, respectively. Excluding the influence of sample dispersion and refractive index selection [24], the peak size of graphite powder particle size distribution should be about 5 μm. The copper particle size (Fig. 1c) was between 20 and 100 μm, and the peak appeared around 40 μm. The particle size of manganese powder (Fig. 1d) ranged from 5 to 60 μm, and the peak value appeared at about 15 μm. As shown in Table 2, the average

particle size (D50) of iron, graphite, copper and manganese powders were 74.082, 3.855, 32.828 and 12.940 μm, respectively. The specific surface area of powder particles decreased with the increase of average particle size.

3.1.2. Morphological characteristics

Scanning electron microscopy was used to observe the morphology of raw material powder. The results are shown in Fig. 2. It could be seen from the figure that water atomized iron powder (Fig. 2a), copper powder (Fig. 2c) and manganese powder atomized (Fig. 2d) were irregular, while natural graphite powder (Fig. 2b) was flaky. At the same time, the results of scanning electron microscopy and particle size distribution test were the same. That is, the particle size of iron powder was about 60 μm, that of graphite powder was about 3 μm, that of copper powder was about 30 μm, and that of manganese powder was about 10 μm.

3.2. Single factor test

3.2.1. Effect of the ball milling time

Milling time is a key parameter, and it directly affects the morphology and distribution of the milled powders. As the ball milling time increases, the powder is gradually refined. However, if the ball milling time is too long, the
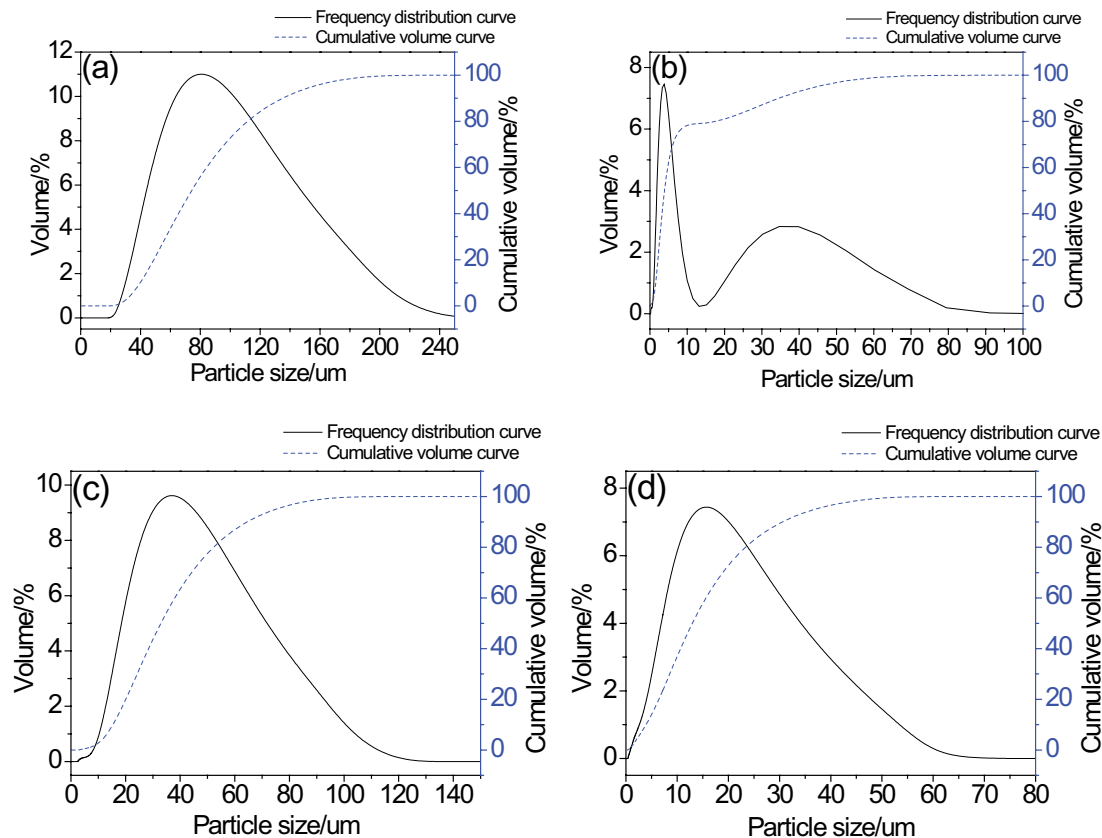
Fig. 1. Powder particle size distribution of raw materials for experiment (a) iron powder, (b) graphite powder, (c) copper powder, (d) manganese powder.

Table 2
Particle size and specific surface area of raw materials for experiment

Raw material	D_{10} (µm)	D_{50} (µm)	D_{90} (µm)	Specific surface area (m²/g)
Iron powder,	39.778	74.082	135.065	0.109
Graphite powder	1.554	3.885	34.465	2.020
Copper powder	15.442	32.828	63.881	0.226
Manganese powder	3.943	12.940	30.297	0.794

powder properties may deteriorate, and at the same time, more impurities increase the contamination of the powder [25]. Therefore, the powder should be properly ground to achieve a good composition to ensure that the powder is in equilibrium between fracture and cold welding [26].

In the early stage of the test, the horizontal value of ball milling time was determined through many exploratory tests. Therefore, under the initial conditions of ball milling speed 300 rpm, absolute ethanol addition 50% (by total powder mass) and ball-to-powder weight ratio 10:1, the effects of ball milling time of 10, 20, 30 and 40 h, respectively, on the particle size and morphology of the powder were investigated. The results are shown in Figs. 3–5.

Fig. 3 shows that with the increase of milling time, the particle size distribution area of the mixed powders first narrowed and moved to the direction of low particle size. When milling time reached 30 and 40 h, the particle size of the powders did not change much. As shown in Fig. 4, D10, D50 and D90 of powder particles decreased rapidly and then stabilized with the increase of milling time. Fig. 5 shows that with the increase of milling time, the mixed powders were refined gradually. When milling time was 30 h (Fig. 5c), the morphology of powders did not change much compared with that of 20 h (Fig. 5b). When the milling time reached 40 h (Fig. 5d), the morphology became more rounded and the particle size distribution became more uniform.

Whether the powder particles are broken during the whole ball milling process is based on whether the grinding balls have an effective collision with the particles. Therefore, the number of effective collisions of the grinding ball is significant for powder refinement. Assuming that the ball milling time is t, the number of effective collisions of the grinding ball can represent N as: $N = kRt/D$ [27], Where R represents the ball-to-powder weight ratio; D represents the radius of the grinding ball; and k is the proportionality
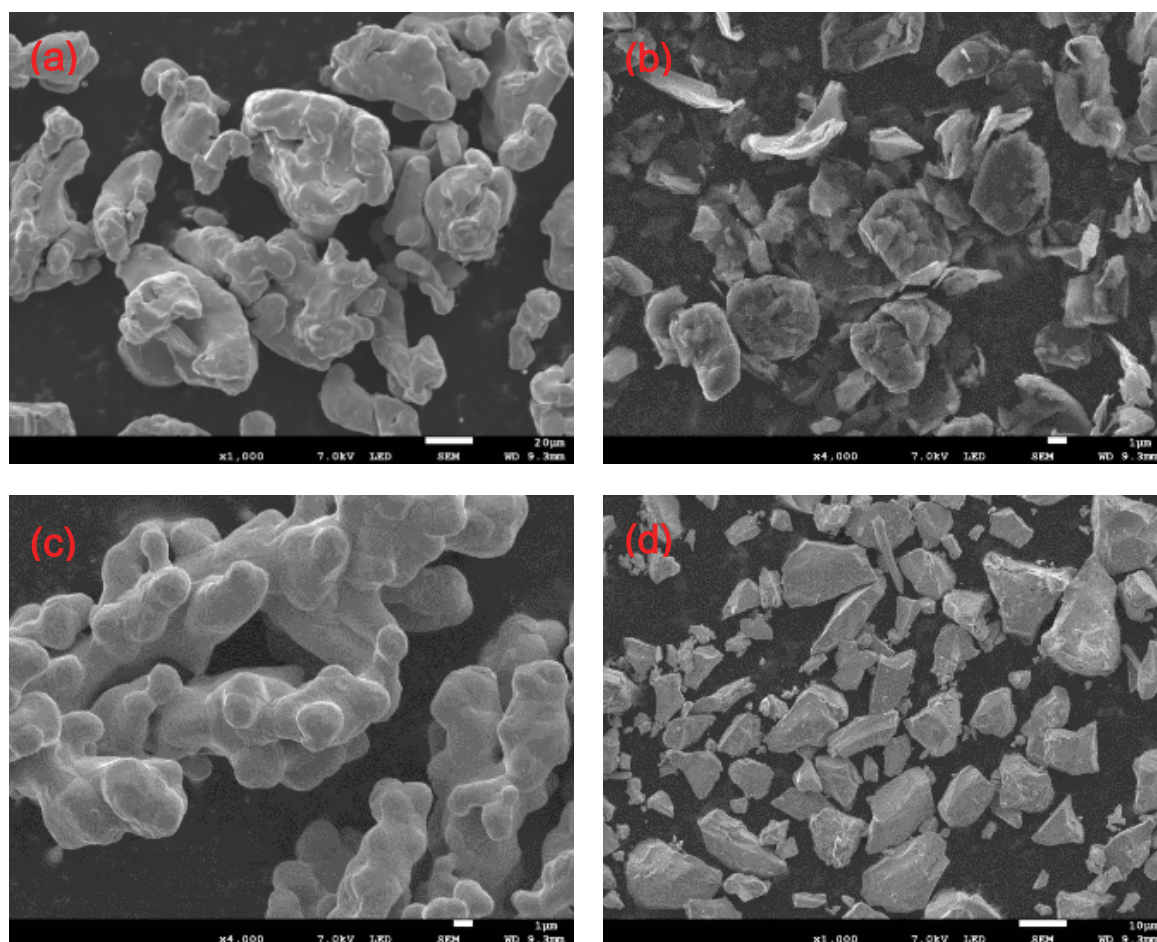
Fig. 2. SEM morphology of raw materials for experiments (a) iron powder × 1,000; (b) graphite powder × 4,000; (c) copper powder × 4,000; (d) manganese powder × 1,000.
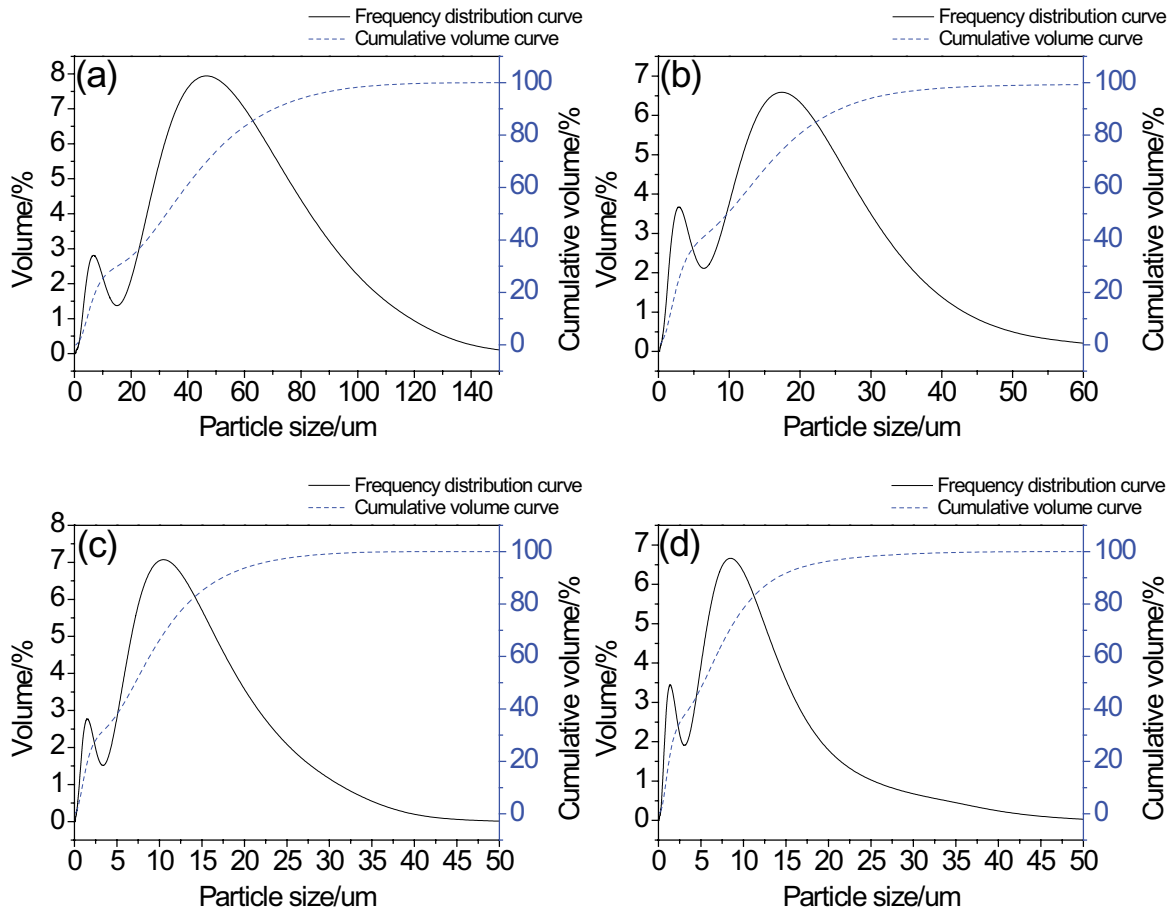
Fig. 3. Powder particle size distribution of different ball milling time (a) 10, (b) 20, (c) 30, (d) 40 h.
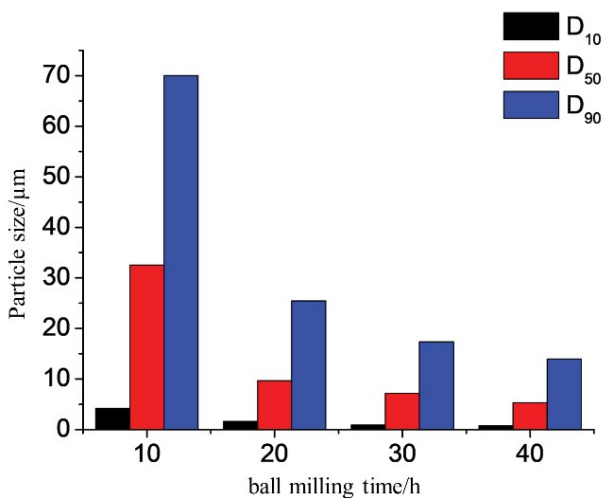
Fig. 4. Variation of particle size of different ball milling time.

factor depending on the characteristics of the grinding ball. According to the formula, when the ball mill and the ball-to-powder weight ratio are fixed, the effective collision number of the grinding ball to the powder is proportional to the ball milling time. In the early stage of ball milling (usually within 1 h), the mixed powders are welded together under the combined action of impact, compression, shear and wear of high-speed grinding balls, and there is no fracture of particles. With the prolongation of ball milling time, the effective collision increases, the effect of cold welding increases sharply, and the stress and strain inside the powder particles increase, resulting in a large number of defects which are easy to induce microcracks. Under the combined action of work hardening, the powder becomes more and more brittle, and gradually breaks into fine particles. After milling for a period of time, the surface energy of grains increases with the decrease of particle size, and agglomeration occurs between grains, which make the grain size larger [28]. Therefore, in the process of continuous deformation, cold welding, crushing and cold welding of mixed powders, when the milling time was 20 h, the dynamic balance between the particle cold welding and fracture was gradually achieved. When the milling time was extended to 30 and 40 h, the particle size of the powder did not change much. This was mainly because when the particles were refined to a certain extent, a large amount of deformation energy had been stored in the powder. At the same time, due to the high strength and hardness of refined particles, the energy required for fracture increased, and the mechanical stress required for further refinement increased accordingly, which made the refinement of powders more difficult [29,30]. Therefore, the optimum milling time was 20 h.
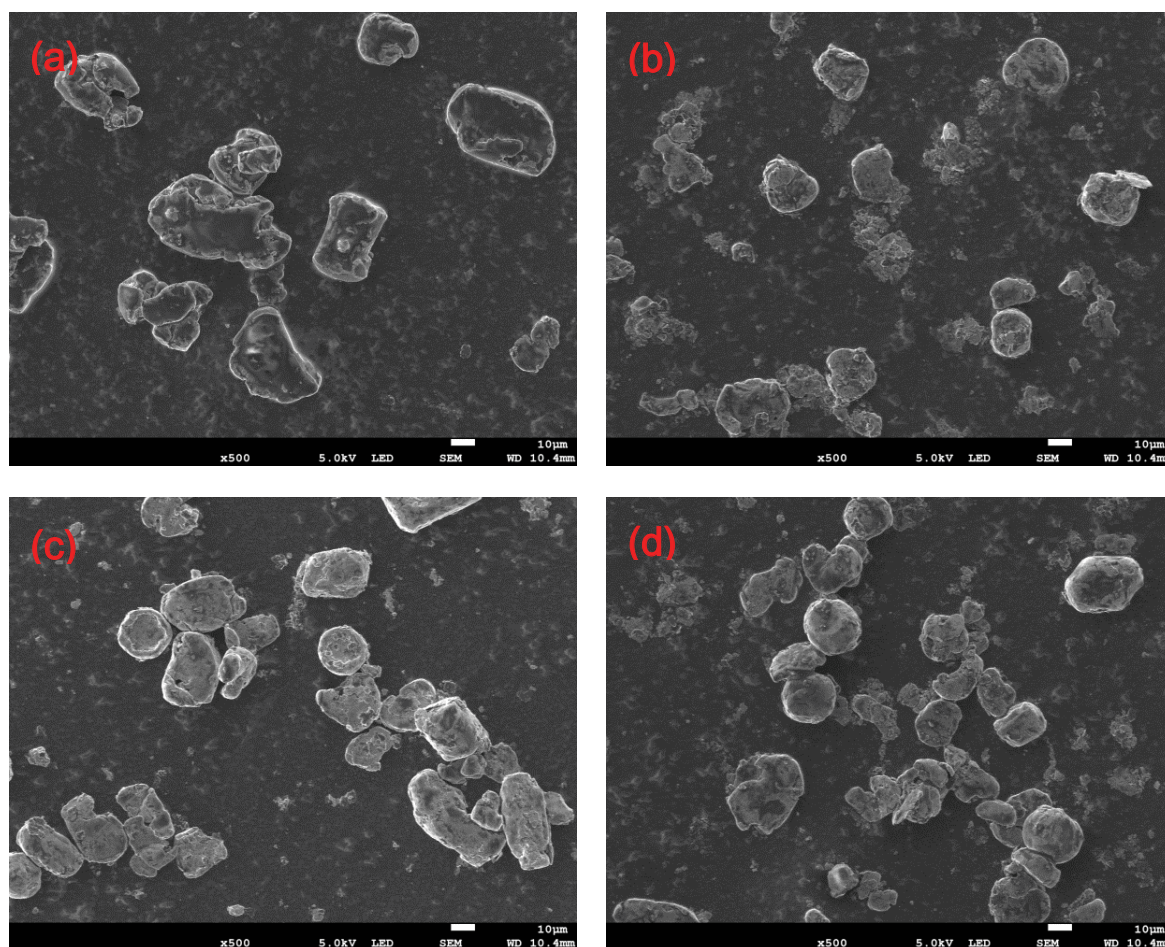
Fig. 5. SEM morphology of different ball milling time (a) Mixed powder 10 h × 500; (b) Mixed powder 20 h × 500; (c) Mixed powder 30 h × 500; (d) Mixed powder 40 h × 500.

3.2.2. Effect of the ball milling speed

Ball milling speed is one of the important variables to be considered in the experiment, which has an important influence on the particle size reduction and morphology [31]. It is generally believed that the higher the rotational speed of the ball milling, the greater the energy obtained by the ball milling powder, which is more conducive to plastic deformation and mechanical alloying of the powder. However, if the ball milling speed is higher than the optimal value, the grinding ball will rotate close to the inner wall of the ball mill tank, thereby reducing the effective collision of the powder and the efficiency of ball milling. At the same time, excessively high rotational speed can cause excessive temperatures in the ball mill tank, causing the decomposition of certain supersaturated solid solutions, amorphous or other metastable phases [32].

In the early stage of the experiment, the horizontal value of the ball milling speed was determined after several exploratory tests. Therefore, under the initial conditions of ball milling time of 20 h, absolute ethanol addition 50% (by total powder mass) and ball-to-powder weight ratio 10:1, the effects of ball milling speeds of 250, 300 and 350 rpm on the particle size and morphology of the powder were investigated. The results are shown in Figs. 6–8.

As shown in Fig. 6, when the ball milling rotation speed was increased from 250 rpm (Fig. 6a) to 300 rpm (Fig. 6b), the particle size distribution region of mixed powder was narrowed and moved toward the low particle diameter direction. When the ball milling speed was 350 rpm (Fig. 6c), the particle size distribution map did not change much compared with 300 rpm. From Fig. 7, it is obvious that the D10, D50 and D90 of the powder particles decreased first and then increased with the increase of ball milling speed. And when the ball milling speed was 300 rpm, the average particle size was the smallest. Fig. 8 shows that when the ball milling speed was increased from 250 rpm (Fig. 8a) to 300 rpm (Fig. 8c), the particle size was remarkably refined. When the ball milling speed was increased to 350 rpm, the particle morphology was more rounded, nearly equiaxed, but the particle size became larger.

As can be seen from the above, as the ball milling speed increased, the particle size first decreased and then increased. As the ball milling speed and the grinding ball movement speed increase, the collision frequency increases, that is, the number of effective collisions is more in a certain period of time. At the same time, during the ball milling process, the force of the powder particles is mainly the impact of the grinding ball on the powder, extrusion, etc. According to
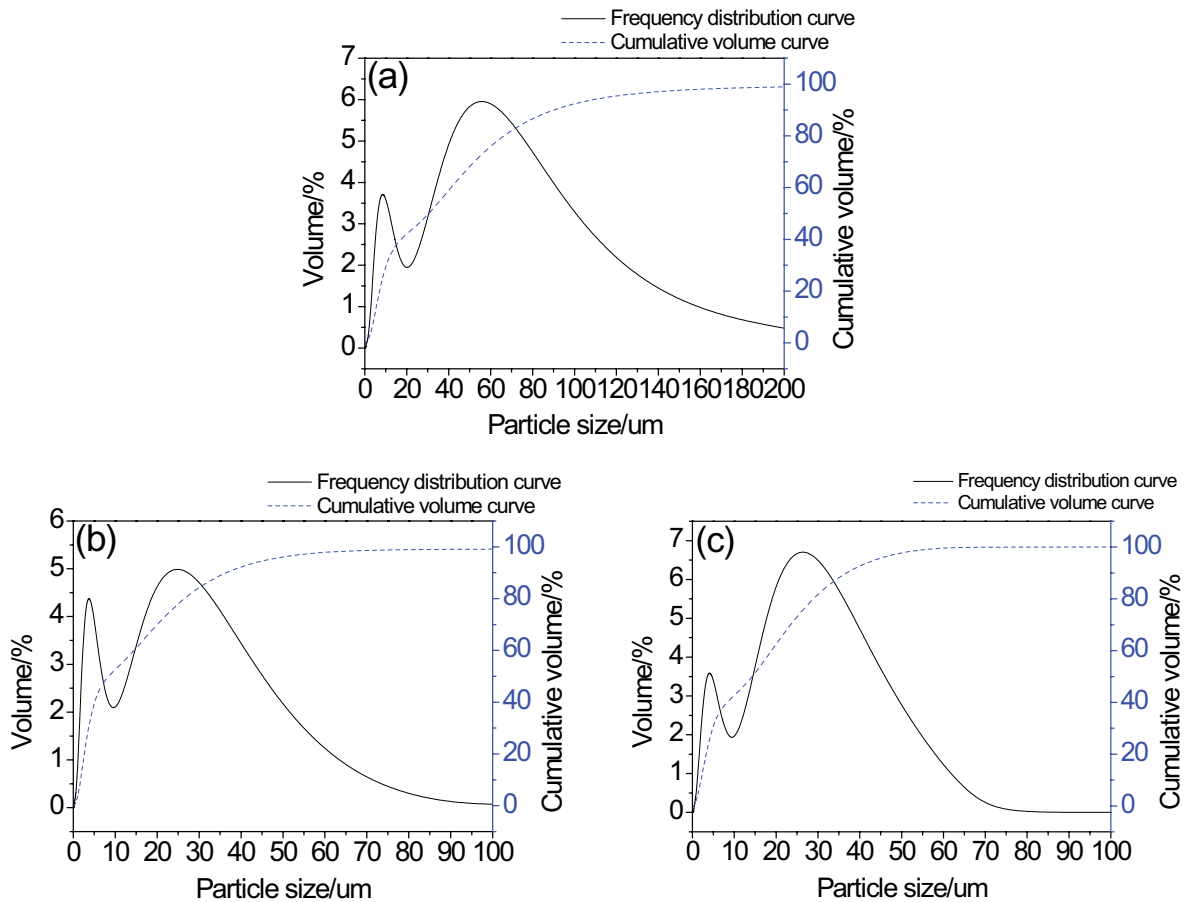
Fig. 6. Powder particle size distribution of different ball milling speeds (a) 250, (b) 300, (c) 350 rpm.
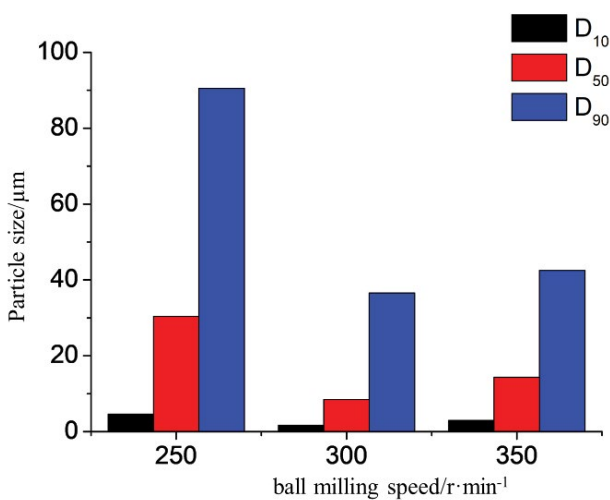
Fig. 7. Variation of particle size of different ball milling speeds.

the kinetic energy theorem, when the speed of the grinding ball increases, the impact force of the powder particles also increases significantly [33]. In two aspects, the powder particles are subjected to severe plastic deformation to be refined. However, the particle diameter of the mixed powder obtained by the ball milling speed of 350 rpm was larger than 300 rpm. This is because during the ball milling process, a part of the powder adhered to the grinding ball and the tank wall, and the other part moved in the tank, which lead to a reduction in effective collision, and the impact energy of the powder particles in different parts to be different, and the magnitude of the conversion into heat energy was also different. Thus, there was a temperature gradient between the powder particles, resulting in a heat transfer phenomenon [34]. The higher the rotational speed, the greater the heat. When the heat was not transferred in time, part of the particle energy was too high, and the atomic diffusion speed was increased, so that the particles were prone to agglomeration and the particle size became larger. Therefore, the optimum ball milling speed was 300 rpm.

3.2.3. Effect of the amount of anhydrous ethanol added

During the ball milling process, as the mixed powder is refined, the surface energy is gradually increased, and agglomeration occurs between the powders to reduce the powder crushing effect and the powder yield. Therefore, a PCA is usually added during the ball milling process. Studies have found that when the amount of PCA is lower or higher, the particle size tends to increase. Most of the PCAs currently used are organic compounds including stearic acid, *n*-hexane, methanol, ethanol and water [13,35–37].
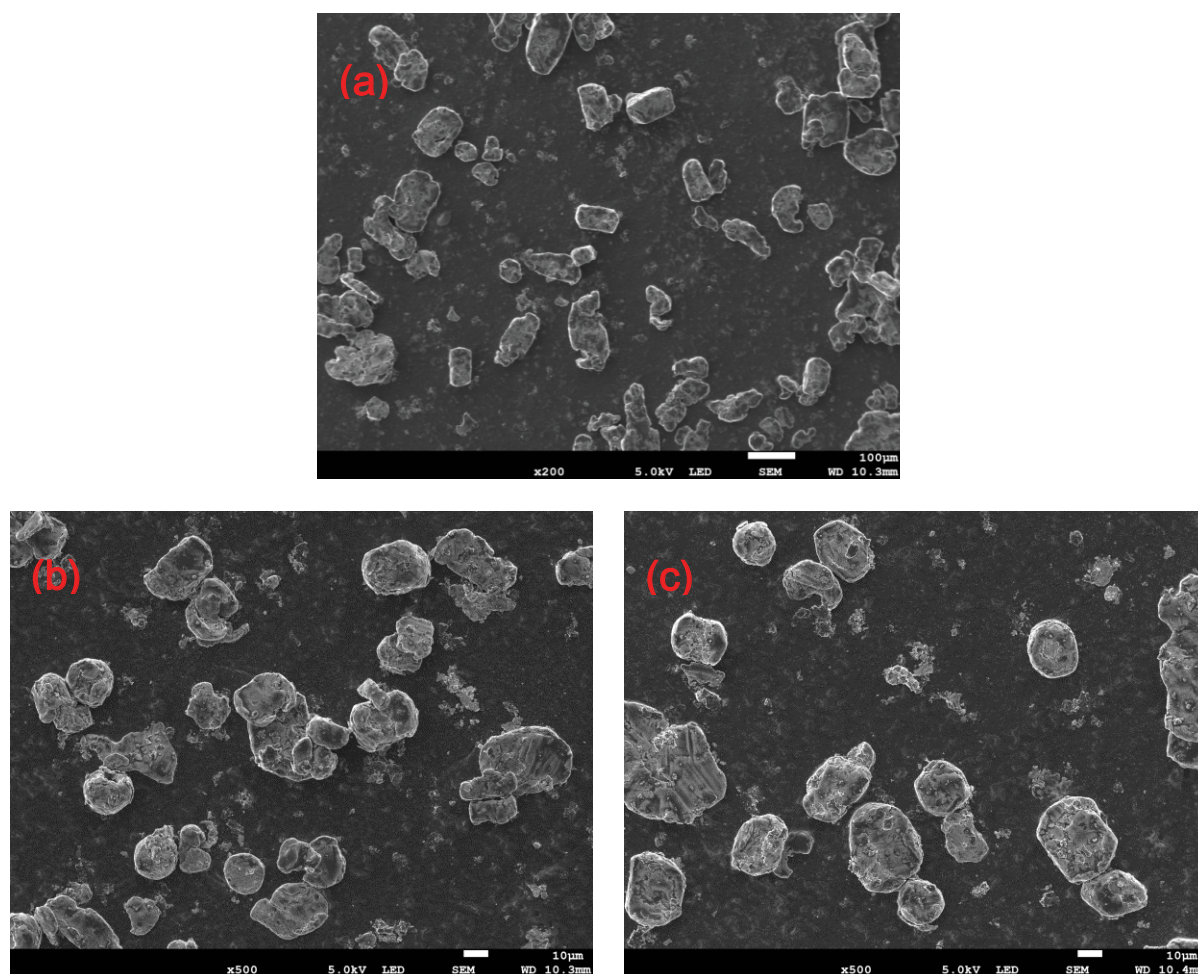
Fig. 8. SEM morphology of different ball milling speeds (a) mixed powder 250 rpm × 200; (b) mixed powder 300 rpm × 500; (c) mixed powder 350 rpm × 500.

Compared with stearic acid, absolute ethanol is good for obtaining finer ball milling powder [38]. Therefore, in this study, anhydrous ethanol was used as a PCA to study the effect of anhydrous ethanol addition (by total powder mass) on the ball milling effect.

On the basis of several exploratory experiments, the horizontal value of the amount of anhydrous ethanol added was finally determined. Therefore, under the initial conditions of ball milling time 20 h, ball milling speed 300 rpm and ball-to-powder weight ratio 10:1, the effects of anhydrous ethanol addition (by total powder mass) of 40%, 50% and 60%, respectively, on the particle size of the powder were investigated. The results were shown in Figs. 9 and 10.

Fig. 9 shows that when the amount of anhydrous ethanol was increased from 40 wt.% (Fig. 9a) to 50 wt.% (Fig. 9b), the particle size distribution region of the mixed powder was narrowed and moved toward the low particle diameter. When the absolute ethanol was added in an amount of 60 wt. % (Fig. 9c), the particle size distribution region and the peak appearance position were slightly shifted to the right by 50 wt.%, and the peak of the large particle size region was significantly larger. From Fig. 10, it is obvious that as the amount of anhydrous ethanol increased, the D10, D50 and D90 of the powder particles first decreased and then increased.

The mixed powder and the grinding ball participated in the ball milling in a more viscous slurry form under the conditions of a suitable amount of anhydrous ethanol added. At this point, the powder tended to adhere to the grinding balls and the wall of the ball mill tank, which increased the chance of the particles being collided and broken by the ball milling media [39]. However, excessive amount of absolute ethanol attenuates the energy transfer of the grinding balls and the ball-milling tank to the powder during the ball milling process, and significantly reduces the rate of particle size refinement. This is why the average particle diameter of the particles became larger when the amount of anhydrous ethanol was increased from 50 wt.% to 60 wt.%. Only when the amount of absolute ethanol added was moderate, a protective film could be uniformly formed on the powder, the wall of the ball mill and the surface of the grinding ball. And this protective film could buffer the energy generated by the collision between the three, adjust the balance between cold welding and crushing, and act as a PCA [37,40]. Therefore, the optimum amount of absolute ethanol added was 50%.
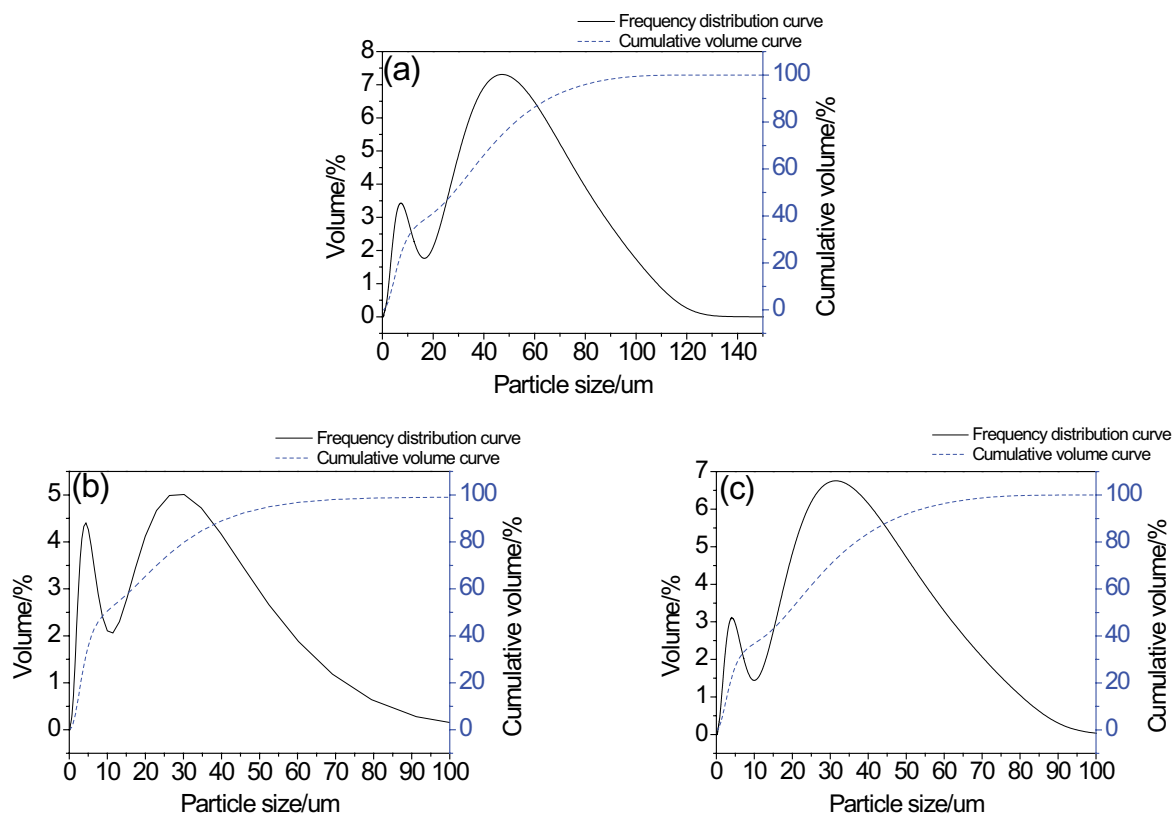
Fig. 9. Powder particle size distribution of different anhydrous ethanol added (a) 40%, (b) 50%, (c) 60%.
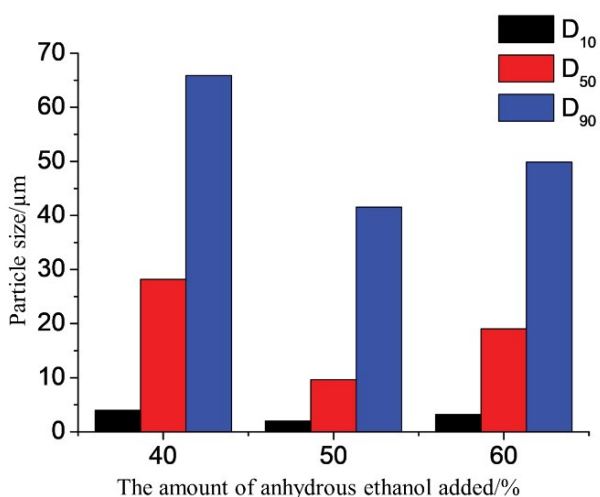
Fig. 10. Particle size variation of powder mixtures having different amounts of anhydrous ethanol.

3.3. Orthogonal test

On the basis of the single factor test, the L18 (37) orthogonal test was designed according to Table 3. The evaluation standard of the orthogonal test was the average particle size (D50) of the mixed powder after ball milling. Through the Minitab15 statistical analysis software, the experimental data were analyzed by Taguchi analysis, analysis of variance and interaction analysis to find out the optimal experimental conditions and the most significant factors affecting the ball milling effect, and to analyze the interaction. The orthogonal test designed and results are shown in Table 4 and Fig. 11.

Fig. 11 shows that the optimum levels of ball milling time, ball milling speed and absolute ethanol addition were A2, B2 and D2 (in Taguchi analysis, the smaller the response mean, the smaller the average particle size), respectively, that is, ball milling time of 20 h, ball milling speed of 300 rpm and absolute ethanol addition amount 50%. The influence of three factors on the ball milling effect was extremely significant (in the analysis of variance, $p < 0.05$). And there were interactions between the three factors (in the interaction analysis, the lines are not parallel).

4. Corrosion properties of internal electrolytic filler

4.1. Corrosion properties of self-made internal electrolytic filler

The potentiodynamic polarization curve is a modern test method for characterizing the corrosion kinetics of metals and their alloys. Measuring the potentiodynamic polarization curve can obtain kinetic information about the corrosion process performed on the corroded metal electrode, including the self-corrosion potential, the corrosion current density, and the Tafel slope of the anodic reaction and the cathodic reaction.

At the time of the test, the potentiodynamic polarization curves of the research electrodes were measured in NaCl

Table 3
Ball milling process orthogonal test factor level

Factors	Levels		
	1	2	3
Ball milling time (h)	10	20	30
Ball milling speed (rpm)	250	300	350
Addition of absolute ethanol (%)	40	50	60

solutions with pH values of 1.0, 3.0, 5.0 and 7.0, respectively, and the results are shown in Fig. 12. The self-corrosion potential E_{coor} and the corrosion current density i_{coor} of the studied electrode were obtained by the Tafel epitaxy method in Fig. 13, and the corrosion rate v of the metal was calculated according to Eq. (1). The results are shown in Table 5.

As shown in Fig. 12, the polarization curves of the working electrode under different pH conditions were composed of a cathode polarization zone and an anode polarization zone. When the polarization potential was less than the self-corrosion potential, cathodic polarization occurred, and the polarization current density increased as the polarization potential increased. When the polarization potential reached the self-corrosion potential, it entered the anode polarization. As the polarization potential increased, the polarization current density increased first, followed by a slowly increasing region, the anode passivation region. The polarization current density at the end of the passivation region continued to increase with the increase of the polarization potential.

In the passivation region, the surface of the filler rapidly formed a passivation film with good corrosion resistance, which reduced the corrosion rate. However, when pH = 1.0, the passivation phenomenon was not obvious. The reason is that when there is no compounding agent or other anion capable of forming a precipitate with metal ions in the solution, the main component of the passivation film of most metals is oxides or hydroxides with low solubility, and these oxides or hydroxides are easily dissolved in strongly acidic solutions [41].

As shown in Table 5, the order of the self-corrosion potential E_{coor} under different pH conditions was: pH 1.0 > pH 5.0 > pH 7.0 > pH 3.0, and the order of corrosion current density i_{coor} was: pH 1.0 > pH 3.0 > pH 5.0 > pH 7.0. According to the corrosion electrochemistry, the more positive the corrosion potential E_{coor}, the smaller the corrosion tendency of the material; the more positive the corrosion current density i_{coor}, the greater the corrosion degree of the material. Therefore, from the viewpoint of corrosion tendency, the research electrode had the highest corrosion tendency in the solution with pH = 3.0, and the corrosion tendency tended to be the smallest in the solution with pH = 1.0, that is, the corrosion tendency of the self-made internal electrolytic filler in weak acidity and neutrality was stronger than that of strong acidity. According to the magnitude of the corrosion current density, the internal electrolytic filler had the fastest corrosion reaction in the solution with pH = 1.0, and the corrosion reaction rate decreased with the increase of the pH value.

In summary, when the electrolyte solution was 3.5 wt.% NaCl solution, the self-made internal electrolytic filler had the fastest corrosion rate in the solution with pH 1.0, but

Table 4
Ball milling orthogonal test design and results

No	A	B	C	D	E	F	G	Average particle size/μm
1	1(10)	1(250)	1(10 × 250)	1(40)	1(10 × 40)	1(250 × 40)	1	45.312
2	1(10)	2(300)	2(10 × 300)	2(50)	2(10 × 50)	2(300 × 50)	2	32.524
3	1(10)	3(350)	3(10 × 350)	3(60)	3(10 × 60)	3(350 × 60)	3	38.716
4	2(20)	1(250)	1(20 × 250)	2(50)	2(20 × 50)	3(250 × 50)	3	30.399
5	2(20)	2(300)	2(20 × 300)	3(60)	3(20 × 60)	1(300 × 60)	1	19.028
6	2(20)	3(350)	3(20 × 350)	1(40)	1(20 × 40)	2(350 × 40)	2	26.845
7	3(30)	1(250)	2(30 × 250)	1(40)	3(30 × 40)	2(250 × 40)	3	28.785
8	3(30)	2(300)	3(30 × 300)	2(50)	1(30 × 50)	3(300 × 50)	1	7.181
9	3(30)	3(350)	1(30 × 350)	3(60)	2(30 × 60)	1(350 × 60)	2	21.348
10	1(10)	1(250)	3(10 × 250)	3(60)	2(10 × 60)	2(250 × 60)	1	85.79
11	1(10)	2(300)	1(10 × 300)	1(40)	3(10 × 40)	3(300 × 40)	2	80.42
12	1(10)	3(350)	2(10 × 350)	2(50)	1(10 × 50)	1(350 × 50)	3	68.92
13	2(20)	1(250)	2(20 × 250)	3(60)	1(20 × 60)	3(250 × 60)	2	43.75
14	2(20)	2(300)	3(20 × 300)	1(40)	2(20 × 40)	1(300 × 40)	3	26.31
15	2(20)	3(350)	1(20 × 350)	2(50)	3(20 × 50)	2(350 × 50)	1	14.314
16	3(30)	1(250)	3(30 × 250)	2(50)	3(30 × 50)	1(250 × 50)	2	48.67
17	3(30)	2(300)	1(30 × 300)	3(60)	1(30 × 60)	2(300 × 60)	3	35.56
18	3(30)	3(350)	2(30 × 350)	1(40)	2(30 × 40)	3(350 × 40)	1	33.62

Note: A = ball milling time/h, B = ball milling speed/rpm, C = ball milling time × ball milling speed/h × rpm, D = the addition of absolute ethanol/%, E = ball milling time × the addition of absolute ethanol/h × %, F = ball milling speed × the addition of absolute ethanol/rpm × %, G = blank column.

Taguchi Analysis: the average particle size versus A. ball milling time, B. ball milling speed, D. the addition of absolute ethanol

Response Table for Means

Level	A. ball milling time	B. ball milling speed	C. the addition of absolute ethanol
1	58.61	47.12	40.22
2	26.77	33.50	33.67
3	29.19	33.96	40.70
Delta	31.84	13.61	7.03
Rank	1	2	3

(a)

General Linear Model: the average particle size versus A. ball milling time, B. ball milling speed, D. the addition of absolute ethanol

Factor	Type	Levels	Values
A. ball milling time	fixed	3	1 (10), 2 (20), 3 (30)
B. ball milling speed	fixed	3	1 (250), 2 (300), 3 (350)
C. the addition of absolute ethanol	fixed	3	1 (20), 2 (25), 3 (30)

Analysis of Variance for the average particle size, using Adjusted SS for Tests

Source	DF	Seq SS	Adj SS	Adj MS	F	P
A. ball milling time	2	3770.2	3770.2	1885.1	6.53	0.013
B. ball milling speed	2	717.3	717.3	358.7	1.24	0.026
C. the addition of absolute ethanol	2	185.1	185.1	92.5	0.32	0.032
Error	11	3174.0	3174.0	288.5		
Total	17	7846.6				

(b)
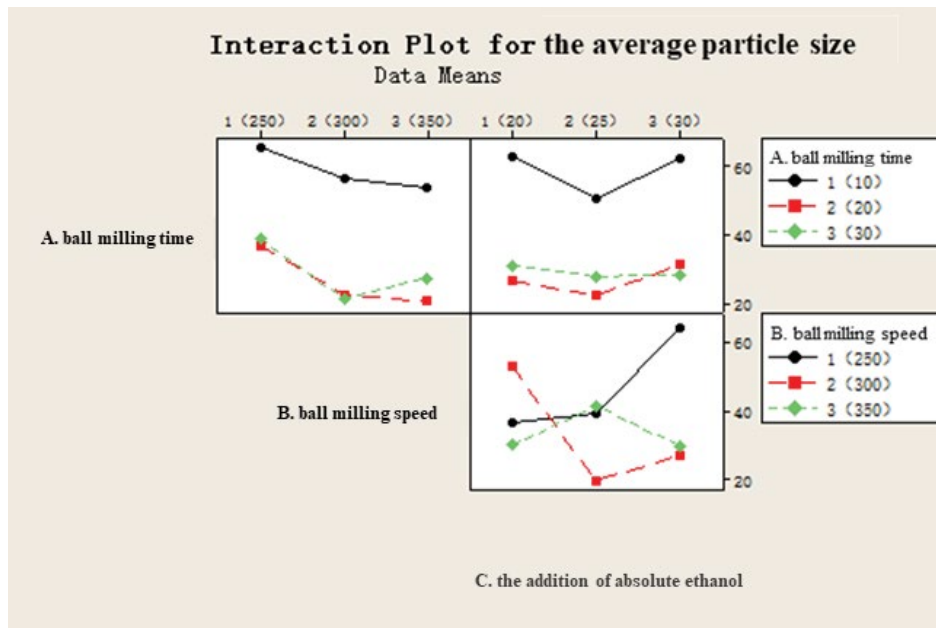
(c)

Fig. 11. Ball milling orthogonal test analysis results (a) Taguchi analysis, (b) analysis of variance, (c) interaction analysis.

the corrosion tendency was the smallest at this time. The corrosion rate in the solution with 3.0 pH was less than 1.0 and greater than 5.0 and 7.0, and at this time, the corrosion tendency was the strongest, and the cation and cathode of the etched microbattery were more likely to undergo redox reaction. If the internal electrolytic filler is used to treat the wastewater and the pH of the wastewater solution is adjusted to 3.0, the reaction rate is faster and the cost is lower (no need to add a large amount of acid to satisfy the strong acidic condition). Therefore, the optimum solution pH of the internal electrolytic treatment wastewater was 3.0.

4.2. Corrosion properties comparison test

The experiment used three internal electrolytic fillers, which were self-made ultrafine grinding catalytic internal electrolytic filler (marked as 1# filler), spherical internal electrolytic filler purchased from Weihua Dick (Beijing)
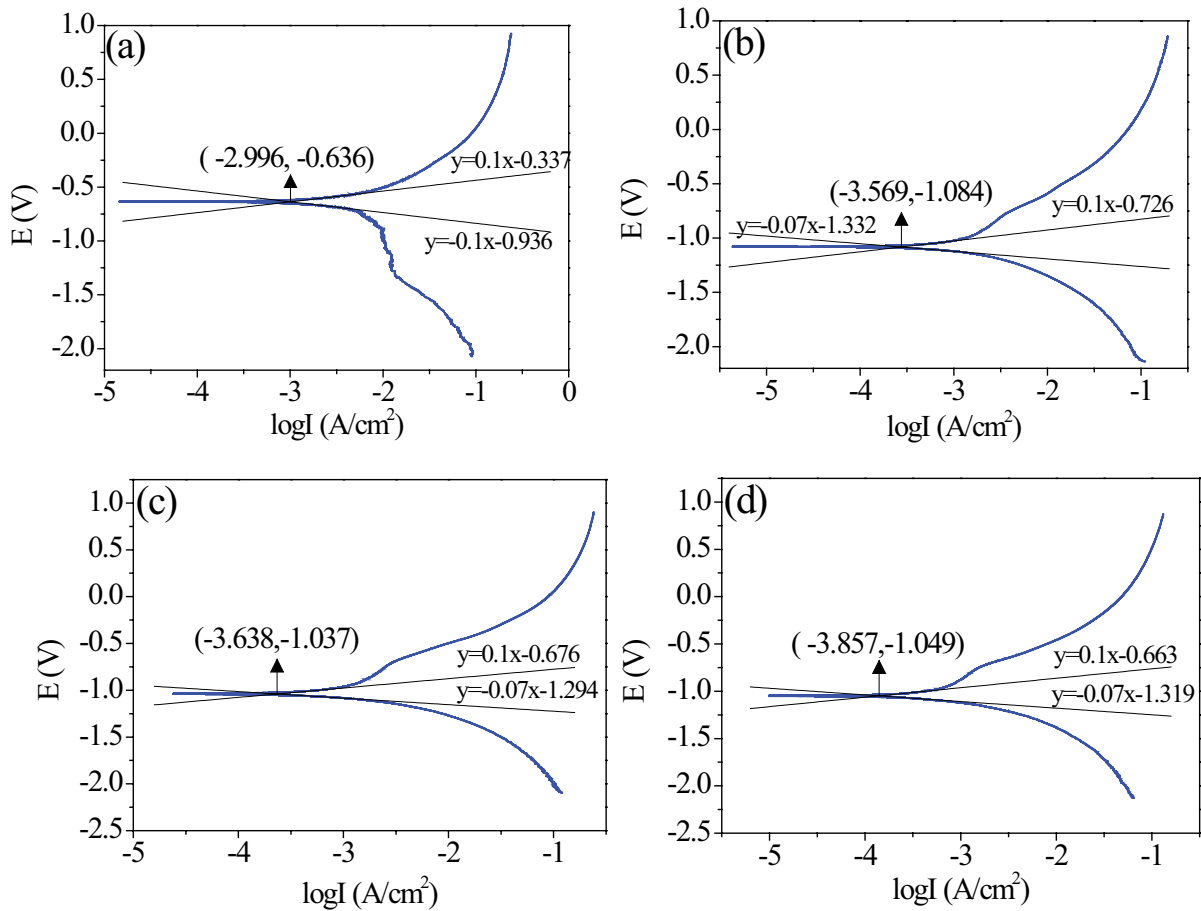
Fig. 12. Potentiodynamic polarization curves of internal electrolytic fillers at different pH values pH 1.0, (b) pH 3.0, (c) pH 5.0, (d) pH 7.0.

Table 5
Electrochemical corrosion parameters of internal electrolytic fillers at different pH values

Solution pH	E_{coor} (V)	i_{coor} (μA/cm^2)	v (g/(m^2 h))
1.0	−0.636	1,009.300	10.541
3.0	−1.084	269.800	2.817
5.0	−1.037	230.100	2.403
7.0	−1.049	138.900	1.451

Fig. 13. Tafel epitaxial method for measuring metal corrosion rate.

Technology Co., Ltd. (marked as 2# filler) and flat spheroidal internal electrolytic filler purchased from Weifang Xinhongyuan Environmental Protection Technology Co., Ltd. (marked as 3# filler). At the time of the test, the potentiodynamic polarization curves of the three study electrodes were measured in NaCl solutions with pH values of 1.0, 3.0, 5.0 and 7.0, respectively, and the results are shown in Fig. 14. Then, according to the Tafel epitaxial method of Fig. 13, the self-corrosion potential E_{coor} and the corrosion current density i_{coor} of the electrode were obtained, and the corrosion rate v was calculated according to Eq. (1). The results are shown in Table 6.

As shown in Table 6, when the pH of the NaCl solution was 1.0 and 7.0, the order of the self-corrosion potential of the three research electrodes was: 2# > 3# > 1#; when the pH was 3.0 and 5.0, the order of the self-corrosion potential was: 3# > 2# > 1#. According to the corrosion kinetics, the larger the self-corrosion potential, the smaller the corrosion tendency. At the four pH values, the self-corrosion potential of the
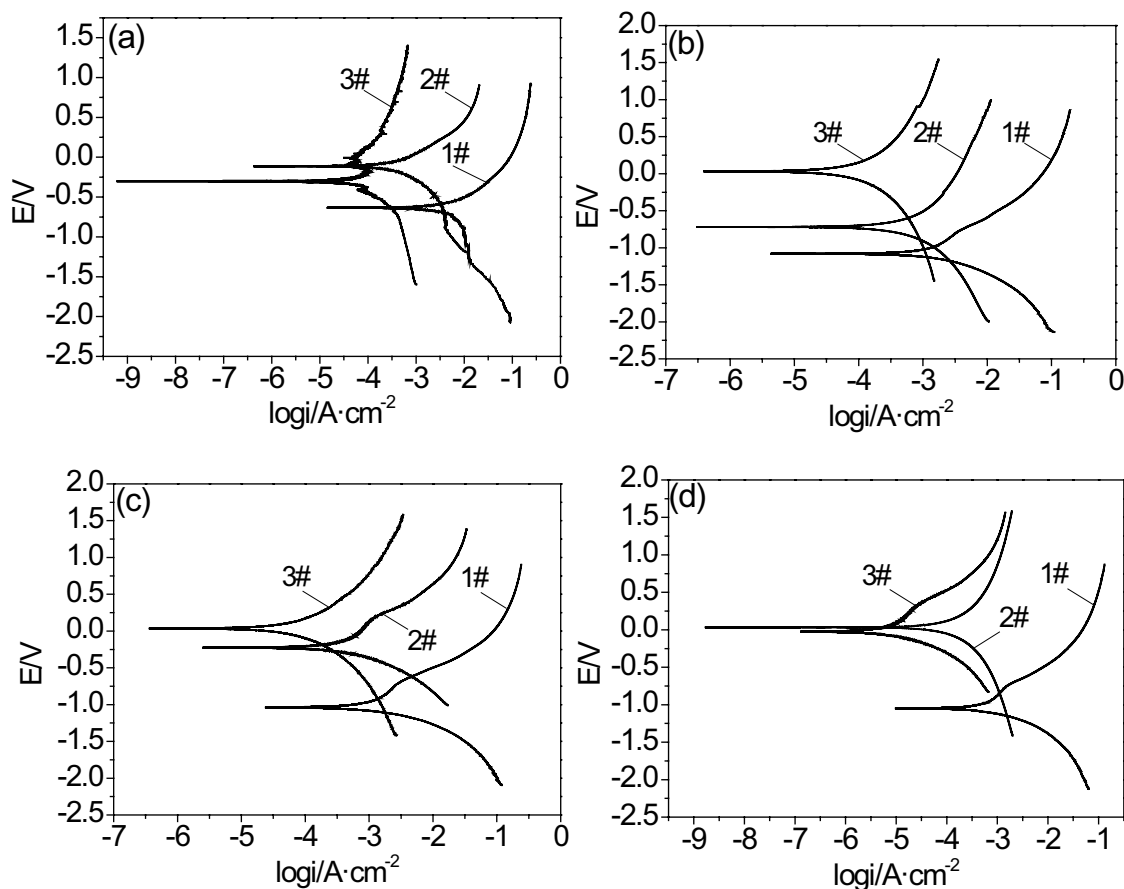
Fig. 14. Potentiodynamic polarization curves of different internal electrolytic fillers (a) pH 1.0, (b) pH 3.0, (c) pH 5.0, (d) pH 7.0.

self-made internal electrolytic filler was the smallest, that is, the corrosion tendency was the largest, and the microbattery reaction was most likely to occur.

Table 6 also shows that under the four pH conditions, the order of the corrosion current density of the three research electrodes was: 1# > 2# > 3#. According to the thermodynamics of corrosion, the higher the corrosion current density, the greater the corrosion degree of the material. That is to say, the self-made internal electrolytic filler had faster corrosion rate and the highest reaction rate than the other two conventional internal electrolytic fillers, and the passivation and compaction phenomenon were alleviated.

5. Conclusion

The subject used the method of PM to prepare ultrafine grinding catalytic internal electrolytic filler. The effects of ball milling time, ball milling speed and absolute ethanol addition on ball milling were investigated by single factor test and orthogonal test. The difference in corrosion performance between self-made internal electrolytic fillers and commercially available conventional internal electrolytic fillers was investigated. Overall, the conclusions could be drawn as follows:

- With the prolongation of the ball milling time, the particle size of the powder particles first decreased rapidly

and then did not change much. With the increase of the ball milling speed and the addition of absolute ethanol, the particle size of the powder particles first decreased and then increased. Under the optimum conditions, when the average particle diameter (D50) of iron powder, graphite powder, copper powder and manganese powder was 74.082, 3.885 32.828 and 12.940 μm, respectively, the average particle diameter of the mixed powder after ball milling was 9.660 μm, and the particle size distribution was uniform and the morphology was round.

- Based on the single factor test, the optimal process conditions for ball milling were obtained by orthogonal test: ball milling time of 20 h, ball milling speed of 300 rpm and absolute ethanol addition of 50% (by total powder mass). The influence of three factors on the ball milling effect was extremely significant, and there were interactions between the three factors.

- The corrosion tendency of self-made internal electrolytic filler under different pH conditions from large to small was: pH 3.0 > pH 7.0 > pH 5.0 > pH 1.0, and the corrosion rate from high to small was: pH 1. 0 > pH 3.0 > pH 5.0 > pH 7.0. The optimum solution pH for treating wastewater using the internal electrolytic filler was 3.0.

- The corrosion tendency of the three research electrodes from large to small was: 1# > 3# > 2# (pH 1.0 and pH 7.0), 1# > 2# > 3# (pH 3.0 and pH 5. 0); The corrosion rate from large to small was: 1# > 2# > 3# (pH 1.0, pH 3.0, pH 5.0,

Table 6
Electrochemical corrosion parameters of different internal electrolytic fillers

(a) pH 1.0

Packing	E_{coor} (V)	log (A/cm^2)	i_{coor} (µA/cm^2)	v (g/(m^2 h)
1#	−0.636	−2.996	1,009.300	10.541
2#	−0.108	−3.758	174.753	1.825
3#	−0.303	−4.545	28.480	0.297

(b) pH 3.0

Packing	E_{coor} (V)	log (A/cm^2)	i_{coor} (µA/cm^2)	v (g/(m^2 h)
1#	−1.084	−3.569	269.800	2.817
2#	−0.719	−3.864	136.887	1.429
3#	0.033	−4.894	12.766	0.133

(c) pH 5.0

Packing	E_{coor} (V)	log (A/cm^2)	i_{coor} (µA/cm^2)	v (g/(m^2 h)
1#	−1.037	−3.638	230.100	2.403
2#	−0.224	−4.354	44.306	0.463
3#	0.036	−5.085	8.225	0.086

(d) pH 7.0

Packing	E_{coor} (V)	log (A/cm^2)	i_{coor} (µA/cm^2)	v (g/(m^2 h)
1#	−1.049	−3.857	138.900	1.451
2#	0.033	−4.864	13.688	0.143
3#	−0.026	−5.618	2.409	0.025

pH 7.0). The self-made internal electrolytic filler had the strongest corrosion tendency and largest reaction rate, and the passivation and compaction were alleviated.

Acknowledgments

References

[1] Y. Ke, I.M.C. Lo, H. Dong, P. Rao, M.S.H. Mak, Lab-scale simulation of the fate and transport of nano zero-valent iron in subsurface environments: aggregation, sedimentation, and contaminant desorption, J. Hazard. Mater., 227–228 (2012) 118–125.

[2] G. Varank, S. Yazici Guvenc, A. Demir, A comparative study of electrocoagulation and electro-Fenton for food industry wastewater treatment: multiple response optimization and cost analysis, Sep. Sci. Technol., 53 (2018) 2727–2740.

[3] M. Sahana, H. Srikantha, S. Mahesh, M.M. Swamy, Coffee processing industrial wastewater treatment using batch electrochemical coagulation with SS and Fe electrodes and its combinations, recovery and reuse of sludge, Water Sci. Technol., 78 (2018) 279–289.

[4] Y. Chang, L. Deng, X. Meng, W. Zhang, C. Wang, Y. Wang, S. Zhao, L. Lin, J.C. Crittenden, Closed-loop electrochemical recycling of spent copper(ii) from etchant wastewater using a carbon nanotube modified graphite felt anode, Environ. Sci. Technol., 52 (2018) 5940–5948.

[5] H. Wang, Q. Gong, H. Huang, T. Gao, Z. Yuan, G. Zhou, P-n heterostructured TiO$_2$/NiO double-shelled hollow spheres for the photocatalytic degradation of papermaking wastewater, Mater. Res. Bull., 107 (2018) 397–406.

[6] X. Zhang, W. Dong, F. Sun, W. Yang, J. Dong, Degradation efficiency and mechanism of azo dye RR2 by a novel ozone aerated internal micro-electrolysis filter, J. Hazard. Mater., 276 (2014) 77–87.

[7] E. Hoseinzadeh, A. Rezaee, M. Farzadkia, Nitrate removal from pharmaceutical wastewater using microbial electrochemical system supplied through low frequency-low voltage alternating electric current, Bioelectrochemistry, 120 (2018) 49–56.

[8] X. Song, M. Liu, Advanced treatment of biotreated coking wastewater with peroxymonosulfate oxidation catalyzed by granular activated carbon, J. Chem. Technol. Biotechnol., 93 (2017) 2191–2198.

[9] J. Luo, G. Song, J. Liu, G. Qian, Z. Xu, Mechanism of enhanced nitrate reduction via micro-electrolysis at the powdered zero-valent iron/activated carbon interface, J. Colloid Interface Sci., 435C (2014) 21–25.

[10] S. Yuan, J. Kang, X. Wu, L. Wang, J. Chen, X. Lu, Development of a novel internal electrolysis system by iron connected with carbon: treatment of nitroaromatic compounds and case of engineering application, J. Environ. Eng., 136 (2010) 975–982.

[11] J. Lu, Y. He, Q. Zhang, J. Wu, Treatment of chemical wastewater by iron-carbon microelectrolysis combined with O/A/O biological process, Ind. Water Treat., 29 (2009) 89–92.

[12] Z. Yan, D. Yin, L. Luo, G. He, Z. Dai, Integrated product and process development of powder metallurgy hub for automotive clutch, Powder Metall., 62 (2019) 247–257.

[13] S. Biyik, Effect of polyethylene glycol on the mechanical alloying behavior of Cu-W electrical contact material, Acta Phys. Polonica A, 134 (2018) 208–212.

[14] S. Biyik, M. Aydin, Fabrication and arc-erosion behavior of ag8sno2 electrical contact materials under inductive loads, Acta Phys. Polonica A, 131 (2017) 339–343.

[15] X. Sun, L. Zhao, G. Ma, P. Jin, Z. Yu, J. Li, Effect of ball milling on the powder characteristics and welding mechanism of Mg$_2$B$_2$O$_5$w/6061Al matrix composite, Mater. Res. Express, 6 (2019) 96507.

[16] S. Biyik, Effect of cubic and hexagonal boron nitride additions on the synthesis of Ag–SnO$_2$ electrical contact material, J. Nanoelectron. Optoelectron., 14 (2019) 1010–1015.

[17] L. Dyckova, P. Komarov, M. Remesova, M. Dycka, K. Dvorak, M. Menelaou, L. Celko, Optimization of molybdenum powder milling parameters, Obrabotka Metallov-Metal Working Mater. Sci., 20 (2018) 109–122.

[18] B.J. Babalola, M.B. Shongwe, A.L. Rominiyi, S.O. Jeje, P.A. Olubambi, A study of nanocrystalline nickel powders developed via high-energy ball milling, Int. J. Adv. Manuf. Technol., 102 (2019) 3657–3665.

[19] L. Pan, G. Lin, J. Wang, A. Wan, X. Xie, Y. Xie, R. Tu, Study of the application of a self-made ultrafine grinding catalytic internal electrolytic filler in pulping wastewater pretreatment, Desal. Wat. Treat., 139 (2019) 133–144.

[20] L.T. Pan, Y. Han, A novel anoxic-aerobic biofilter process using new composite packing material for the treatment of rural domestic wastewater, Water Sci. Technol., 73 (2016) 2486.

[21] L.-t. Pan, H. Yue, J.-f. Wu, Advanced treatment of biologically pretreated coking wastewater by intensified zero-valent iron process (IZVI) combined with anaerobic filter and biological aerated filter (AF/BAF), J. Central South Univ., 22 (2015) 3781–3787.

[22] L. Pan, J. Wang, W. Wang, J. Wu, B. Yu, Preparation method of iron carbon micro electrolysis filler, CN:200910198816[P], 2011.12.07.

[23] M. Li, Q. Cai, Y. Liu, Z. Ma, Z. Wang, Microstructure and mechanical properties of Ti$_2$AlNb-based alloys synthesized by spark plasma sintering from pre-alloyed and ball-milled powder, Adv. Eng. Mater., 20 (2017) 1700659.

[24] L. Wang, H. Sun, Application research of laser particle size analyzer for measuring fenofibe size distribution, Chin. Antibiot. J., 41 (2016) 675–679.

[25] L. Zhang, Z. Huang, Y. Liu, Y. Shen, K. Li, Z. Cao, Z. Ren, Y. Jian, Effects of mechanical ball milling time on the microstructure and mechanical properties of Mo_2NiB_2-Ni cermets, Materials, 12 (2019) 1926.

[26] Y. Shen, Z. Huang, L. Zhang, Effect of milling time on the microstructure and mechanical properties of Mo_2FeB_2 based cermets, Mater. Res. Express, 4 (2017) 106518.

[27] S. Zhuang, B.B. Nunna, J.A. Boscoboinik, E.S. Lee, Nitrogen-doped graphene catalysts: high energy wet ball milling synthesis and characterizations of functional groups and particle size variation with time and speed, Int. J. Energy Res., 41 (2017) 2535–2554.

[28] X. Ding, D. Yi, B. Wang, P. Yu, W. Cheng, Effects of TiC particles and its surface nickel plating on microstructure sintering properties of sintered H13 steel, Mater. Sci. Eng. Powder Metal., 19 (2014) 940–947.

[29] Z. Yuan, Z. Jin, R. Kang, Q. Wen, Tribochemical polishing CVD diamond film with FeNiCr alloy polishing plate prepared by MA-HPS technique, Diamond Related Mater., 21 (2012) 50–57.

[30] M.F. De Oliveira, G.A. Almyras, G.A, Evangelakis. Structural differences of amorphous Cu 65 Zr 35 between rapidly quenched and topologically destabilized crystalline Cu and Zr metals by molecular dynamics simulations, Comput. Mater. Sci., 104 (2015) 92–97.

[31] S. Biyik, M. Aydin, The effect of milling speed on particle size and morphology of Cu25W composite powder, Acta Phys. Polonica A, 127 (2015) 1255–1260.

[32] A.L. Amigã, C.R.M. Afonso, V. Amigã, Effect of Fe addition on microstructure and properties of powder metallurgy Ti35Nb10Ta alloy, Mater. Sci. Forum, 899 (2017) 206–211.

[33] H.S. Kim, B. Madavali, T.J. Kim, C.M. Kim, J.M. Koo, T.H. Lee, S.J. Hong, Effect of different mechanical milling processes on morphology and microstructural changes of nano and micron Al-powders, Arch. Metal. Mater., 60 (2015) 1235–1239.

[34] A. Canakci, T. Varol, C. Nazik, Effects of amount of methanol on characteristics of mechanically alloyed $Al-Al_2O_3$ composite powders, Mater. Process. Report, 27 (2014) 320–327.

[35] T. Yang, X.-P. Guo, Mechanical alloying behaviors of Mo–Si–B-based alloy from elemental powders under different milling conditions, Rare Metals, 38 (2019) 653–664.

[36] S. Biyik, M. Aydin, Optimization of mechanical alloying parameters of Cu25W electrical contact material, Acta Phys. Polonica A, 132 (2017) 909–912.

[37] V. Mihalache, I. Mercioniu, A. Velea, P. Palade, Effect of the process control agent in the ball-milled powders and SPS-consolidation temperature on the grain refinement, density and Vickers hardness of Fe14Cr ODS ferritic alloys, Powder Technol., 347 (2019) 103–113.

[38] H. Song, Y. Wu, C. Tang, J. Liang, Effect of process control agent on properties of mechanically alloyed Fe-48Al powder, Mater. Eng., 10 (2007) 62–66.

[39] L. Zhang, G. Xiping, Microstructural evolution, thermal stability and microhardness of the Nb–Ti–Si-based alloy during mechanical alloying, Metals, 8 (2018) 403.

[40] C.A. Leónpatiño, D. Ramírezvinasco, E.A. Aguilarreyes, Densi-fication study of Cu-Al-SiC composite powders prepared by mechanical milling, Mater. Sci. Forum, 793 (2014) 37–44.

[41] J. Wang, S. Qian, Y. Liu, Y. Sun, Y. Jiang, J. Li, Crevice corrosion performance of 436 ferritic stainless steel studied by different electrochemical techniques in sodium chloride solutions with sulfate addition, Acta Metallurgica Sinica, 8 (2018) 815–822.